



Article scientifique

Article

2022

Published version

Open Access

This is the published version of the publication, made available in accordance with the publisher's policy.

Simulations of electric field gradient fluctuations and dynamics around sodium ions in ionic liquids

Gimbal-Zofka, Yann Gaël; Karg, Béatrice; Dziubinska-Kühn, Katarzyna; Kowalska, Magdalena; Wesolowski, Tomasz Adam; Rumble, Christopher Allen

How to cite

GIMBAL-ZOFKA, Yann Gaël et al. Simulations of electric field gradient fluctuations and dynamics around sodium ions in ionic liquids. In: The Journal of chemical physics, 2022, vol. 157, n° 24, p. 1–11. doi: 10.1063/5.0126693

This publication URL: <https://archive-ouverte.unige.ch/unige:180183>

Publication DOI: [10.1063/5.0126693](https://doi.org/10.1063/5.0126693)

Simulations of electric field gradient fluctuations and dynamics around sodium ions in ionic liquids

Cite as: J. Chem. Phys. 157, 244502 (2022); doi: 10.1063/5.0126693

Submitted: 16 September 2022 • Accepted: 1 December 2022 •

Published Online: 22 December 2022









View Online



Export Citation



CrossMark

Yann Gimbal-Zofka,¹  Beatrice Karg,²  Katarzyna Dziubinska-Kühn,^{3,4,a)}  Magdalena Kowalska,³ 
Tomasz A. Wesolowski,¹  and Christopher A. Rumble^{5,b)} 

AFFILIATIONS

¹Département de Chimie Physique, Université de Genève, 30, quai Ernest-Ansermet, CH-1211 Genève 4, Switzerland

²Département de Physique Nucléaire et Corpusculaire, Université de Genève, CH-1211 Genève 4, Switzerland

³Experimental Physics Department, CERN, CH-1211 Geneva 23, Switzerland

⁴Institute of Analytical Chemistry, University of Leipzig, D-04103 Leipzig, Germany

⁵The Pennsylvania State University - Altoona College, 3000 Ivyside Park, Altoona, Pennsylvania 16601, USA

^{a)}Current address: Maastricht Center for Systems Biology, 6229 EN Maastricht, Netherlands.

^{b)}Author to whom correspondence should be addressed: crumble@psu.edu

ABSTRACT

The T_1 relaxation time measured in nuclear magnetic resonance experiments contains information about electric field gradient (EFG) fluctuations around a nucleus, but computer simulations are typically required to interpret the underlying dynamics. This study uses classical molecular dynamics (MD) simulations and quantum chemical calculations, to investigate EFG fluctuations around a Na^+ ion dissolved in the ionic liquid 1-ethyl 3-methylimidazolium tetrafluoroborate, $[\text{Im}_{21}][\text{BF}_4]$, to provide a framework for future interpretation of NMR experiments. Our calculations demonstrate that the Sternheimer approximation holds for Na^+ in $[\text{Im}_{21}][\text{BF}_4]$, and the anti-shielding coefficient is comparable to its value in water. EFG correlation functions, $C_{\text{EFG}}(t)$, calculated using quantum mechanical methods or from force field charges are roughly equivalent after 200 fs, supporting the use of classical MD for estimating T_1 times of monatomic ions in this ionic liquid. The EFG dynamics are strongly bi-modal, with 75%–90% of the de-correlation attributable to inertial solvent motion and the remainder to a highly distributed diffusional processes. Integral relaxation times, $\langle\tau_{\text{EFG}}\rangle$, were found to deviate from hydrodynamic predictions and were non-linearly coupled to solvent viscosity. Further investigation showed that Na^+ is solvated by four tetrahedrally arranged $[\text{BF}_4]^-$ anions and directly coordinated by ~ 6 fluorine atoms. Exchange of $[\text{BF}_4]^-$ anions is rare on the 25–50 ns timescale and suggests that motion of solvent-shell $[\text{BF}_4]^-$ is the primary mechanism for the EFG fluctuations. Different couplings of $[\text{BF}_4]^-$ translational and rotational diffusion to viscosity are shown to be the source of the non-hydrodynamic scaling of $\langle\tau_{\text{EFG}}\rangle$.

Published under an exclusive license by AIP Publishing. <https://doi.org/10.1063/5.0126693>

I. INTRODUCTION

Ionic liquids (ILs) are a class of solvents whose unique chemical and physical properties have made them targets for a broad set of applications, ranging from synthesis to energy science, photochemistry, green chemistry, and food science.^{1–10} Among the vast array of experimental and computational techniques used to study the solute and solvent dynamics in ILs, nuclear magnetic resonance (NMR) T_1 relaxation measurements, combined with molecular dynamics simulations, stand out as powerful tools for studying equilibrium and dynamical processes in these systems.¹¹ For nuclei with spin $I \geq 1$ and a sufficiently small gyromagnetic ratio, NMR T_1 relaxation

measurements report directly on the fluctuations of the electric field gradient (EFG) experienced by a nucleus due to solvent fluctuations and the rotation of chemical bonds about the nucleus in question. In particular, T_1 measurements of atoms in molecules provide information about the reorientation of solute molecules, and can be used to sense the mobility of a solute in its local environment. Such measurements have been used extensively in studies of solute dynamics in ionic liquids, as well as for probing the motion of solvent ions themselves.^{12–22}

Solvated monatomic ions, such as Na^+ , Ca^{2+} , and Cl^- have no chemical bonds to rotate about their nucleus; therefore, the EFG dynamics at these nuclei are a consequence of only the

fluctuating solvent. Much effort has been made to understand EFG fluctuations around monatomic ions in water,^{23–36} and this body of work demonstrates that EFG fluctuations are the product of a subtle interplay between collective solvent rotations and translations, where no single solvent motion drives the dynamics. The dynamics of monatomic ions in ionic liquids are of particular interest, due to recent efforts toward the development of sodium-ion batteries using ionic liquid electrolytes;^{37–42} however, NMR T_1 studies of monatomic ions in ILs are rare and have focused primarily on Li^+ .^{43–46} The goal of the present report is to develop a protocol for simulating EFG dynamics around monatomic ions in ionic liquids, for future analysis of T_1 measurements and to investigate which solvent motions are correlated with the EFG dynamics.

In the case of an isotropic system in the extreme narrowing limit, the T_1 relaxation time of a quadrupolar nucleus can be calculated according to Refs. 25, 36, and 47:

$$T_1^{-1} = \frac{1}{20} \frac{2I+3}{I^2(2I-1)} \left(\frac{eQ}{\hbar} \right)^2 \int_0^\infty \langle \mathbf{V}(0) : \mathbf{V}(t) \rangle dt, \quad (1)$$

where I is the nuclear spin, Q the quadrupole coupling constant, $\mathbf{V}(t)$ the EFG tensor at the position of the nucleus at time t , and e and \hbar the elementary charge and reduced Planck's constant. The term $\langle \mathbf{V}(0) : \mathbf{V}(t) \rangle$ is the EFG tensor correlation function and is calculated from

$$\begin{aligned} \langle \mathbf{V}(0) : \mathbf{V}(t) \rangle &= \left\langle \sum_{\alpha\beta} V_{\alpha\beta}(0) V_{\alpha\beta}(t) \right\rangle, \\ &= \left\langle \sum_{\alpha\beta} V_{\alpha\beta}^2 \right\rangle C_{\text{EFG}}(t), \\ &= \langle \mathbf{V}^2 \rangle C_{\text{EFG}}(t), \end{aligned} \quad (2)$$

where the sum runs over the Cartesian axes α and β . Combining Eqs. (1) and (2), we can express the T_1 relaxation time as

$$T_1^{-1} = \frac{1}{20} \frac{2I+3}{I^2(2I-1)} \left(\frac{eQ}{\hbar} \right)^2 \langle \mathbf{V}^2 \rangle \langle \tau_{\text{EFG}} \rangle, \quad (3)$$

where $\langle \tau_{\text{EFG}} \rangle = \int_0^\infty C_{\text{EFG}}(t) dt$ is the integral, or average, EFG correlation time. It is important to note that T_1 times measured in the extreme narrowing region only report on the integral time of the EFG, and insight into the underlying dynamics is lost. Molecular dynamics (MD) simulations and quantum chemical calculations must be used to recover this information.^{18,19,23–26,29,30,34–36}

Predicting T_1 times using computational methods can be a daunting task, as such predictions require accurate descriptions of both the static properties of the EFG, $\langle \mathbf{V}^2 \rangle$, as well as its dynamics, $C_{\text{EFG}}(t)$. In a world of infinite computing power, *ab initio* molecular dynamics simulations would be able to provide direct access to both the magnitude and dynamics of the EFG at the nucleus in question with high chemical accuracy. Such calculations have been attempted for monatomic ions in water,^{29,33,36} but the sluggish dynamics of ILs and requisite long trajectories render such simulations prohibitively expensive and necessitate the use of classical force fields for simulation of the solvent dynamics. The EFG can be calculated from classical MD simulations either directly from the

solvent point charges of the force field or from a quantum mechanical calculation performed at each step of the simulation. The force field approach is preferred due to its low computational cost, but it ignores the contribution of the solute ion's electrons to the EFG. The Sternheimer approximation^{48,49} is used to account for this, which asserts that the total EFG at a nucleus, \mathbf{V} , is linearly related to the external EFG generated by the solvent, \mathbf{V}_{ext} :

$$\mathbf{V} = (1 + \gamma) \mathbf{V}_{\text{ext}}, \quad (4)$$

where γ is the Sternheimer anti-shielding coefficient. One can access \mathbf{V} from a quantum mechanical calculation on a particular simulation frame and \mathbf{V}_{ext} from the “classical” evaluation of the EFG using solvent point charges. The value of γ is then determined by fitting correlation plots of \mathbf{V} vs \mathbf{V}_{ext} . In this work, we will refer to quantum mechanical calculations of the full EFG \mathbf{V} as \mathbf{V}_{QM} , and the solvent-only point-charge evaluation of \mathbf{V}_{ext} as \mathbf{V}_{CL} , which allows us to rewrite Eq. (4) as

$$\mathbf{V}_{\text{QM}} = (1 + \gamma) \mathbf{V}_{\text{CL}}. \quad (5)$$

Sternheimer anti-shielding coefficients have been determined for a number of ions and environments^{50–53} and were recently studied in detail for monatomic ions in water by Chubak and co-workers.³⁶ This study found that γ was not only ion-dependent, as expected, but varied based on the choice of water force field, due to differences in the local solvent structure around the ions. To our knowledge, the Sternheimer approximation has not yet been tested in ionic liquids, which are highly charged relative to dipolar liquids and are known to have heterogeneous local structure.

In the present report, we will test the applicability of the Sternheimer approximation for Na^+ in a prototypical ionic liquid, 1-ethyl 3-methylimidazolium tetrafluoroborate, $[\text{Im}_{21}][\text{BF}_4]$, using density functional theory (DFT) calculations on $\text{Na}^+[\text{Im}_{21}][\text{BF}_4]$ configurations generated by classical MD simulations. After confirmation of the Sternheimer approximation, we will use the MD simulations to examine the solvent dynamics responsible for EFG fluctuations in this system. Through this work, we hope to be able to provide a framework for simulating T_1 times for monatomic ions in ionic liquids for future interpretation of NMR experiments.

II. METHODS

A. Molecular dynamics simulations

The GROMACS 2021.3 package⁵⁴ was used for all molecular dynamics simulations, and the $[\text{Im}_{21}][\text{BF}_4]$ force field parameters were taken from the all-atom force field of Pádúa and Lopes.^{55,56} The system consisted of 200 $[\text{Im}_{21}]^+$ cations, 201 $[\text{BF}_4]^-$ anions, and one Na^+ cation in a cubic box, with periodic boundary conditions constructed using the PACKMOL⁵⁷ and `fftool`⁵⁸ programs. Integration was handled using the Verlet leap-frog algorithm, non-bonded interactions were calculated using a Verlet neighbor list with a cutoff of 1.2 nm, and long-range electrostatic interactions were handled using the smoothed particle-mesh Ewald method.⁵⁹ The solvent model was fully flexible, with the exception of hydrogen-containing bonds, which were fixed using the P-LINCS algorithm.⁶⁰

Simulations were conducted at four temperatures: 298, 350, 400, and 500 K. In all cases, equilibration began with a steepest-descent energy minimization procedure, followed by a 50 ps simulation in the NVT ensemble at 500 K, controlled using the modified Berendsen thermostat,⁶¹ with a relaxation time of 0.1 ps. Next, a 200 ps simulation was carried out in the NPT ensemble at 500 K, which allowed the system to relax to its natural volume. The pressure was controlled in these simulations using a Berendsen barostat, with a relaxation time of 1 ps. For the 500 K trajectory, the box volume was fixed to the average volume of the last 10 ps of the NPT simulation, followed by a final NVT equilibration simulation at 500 K. A production simulation was then performed, with coordinates saved every 0.01 ps for later evaluation of the EFG. Simulations at 400, 350, and 298 K followed a similar procedure, but with extra 5 ns NPT simulations in 50–100 K intervals, until the target temperature was reached. The side lengths of the simulation boxes were 3.728 03 nm at 298 K, 3.763 70 nm at 350 K, 3.805 38 nm at 400 K, and 3.894 31 nm at 500 K. Production simulations were 25 ns long for the 500, 400, and 350 K systems and 50 ns for 298 K. For the EFG calculations, each trajectory was then centered around the Na⁺ ion, with solvent atoms kept whole and wrapped, while preserving periodic boundary conditions.

B. EFG evaluation

EFG tensors were calculated in two ways: using the solvent force field point-charges and classical EFG expression (CL), or with a multi-level quantum mechanical (QM) calculation. For the CL calculations, the contribution of each solvent atom *i* to the EFG tensor at the position of the Na⁺ nucleus was calculated according to

$$\mathbf{V}_i^{(\text{CL})} = A_i \begin{pmatrix} -2x_i^2 + y_i^2 + z_i^2 & -3x_i y_i & -3x_i z_i \\ -3x_i y_i & x_i^2 - 2y_i^2 + z_i^2 & -3y_i z_i \\ -3x_i z_i & -3y_i z_i & x_i^2 + y_i^2 - 2z_i^2 \end{pmatrix}, \quad (6)$$

$$A_i = -\frac{Q_i}{4\pi\epsilon_0} \frac{1}{(x_i^2 + y_i^2 + z_i^2)^{5/2}},$$

where Q_i is the charge on solvent atom *i* and x_i , y_i , and z_i are the Cartesian positions of the solvent atom relative to Na⁺. The contributions of all solvent atoms in the frame are summed, to determine the total EFG tensor at the position of the Na⁺ nucleus:

$$\mathbf{V}_{\text{CL}} = \sum_i \mathbf{V}_i^{(\text{CL})}. \quad (7)$$

These calculations were performed on 50 ns simulations, with varying system sizes—100, 200, and 300 [Im₂₁][BF₄] pairs (Fig. S-1)—to check for consistency. We found that probability distributions of \mathbf{V}_{CL} were indistinguishable for the 200 and 300 ion pair systems; therefore, all simulations were performed with 200 ion pairs, to maximize computational efficiency.

A multi-level quantum mechanical evaluation of the EFG was also performed using a development version of the Q-Chem package.⁶² The quantum mechanical region was constructed from the Na⁺ cation, all [BF₄][−] with F atoms within 4.6 Å of Na⁺, and enough of the nearest [Im₂₁]⁺ ions to create a charge-neutral cluster. We found that there were either 3, 4, or 5 [BF₄][−] within this cutoff, with 99.5% of the simulation frames having 4. This

resulted in a QM region containing 316, 418, or 520 electrons for systems with 3, 4, or 5 [Im₂₁][BF₄] pairs, respectively. The Perdew–Burke–Ernzerhof (PBE) exchange correlation functional⁶³ and the cc-pCVTZ Dunning-type basis were used for all electron DFT based calculations.⁶⁴ To properly describe the electron density near the nucleus, the basis set includes core-polarized functions, as recommended in the literature for EFG calculations.^{28,65} Given the small masses of the nuclei in the system, no relativistic effects were considered. The contribution of all remaining [Im₂₁][BF₄] ions was calculated using the force field charges and Eq. (6).

III. RESULTS

A. Sternheimer anti-shielding coefficients

We begin by determining the Sternheimer anti-shielding coefficient for Na⁺ in [Im₂₁][BF₄], by fitting correlation plots of \mathbf{V}_{CL} vs \mathbf{V}_{QM} from 1000 simulation frames sampled in 25 ps intervals across the MD trajectory. The correlation plots and corresponding fits to Eq. (5) are shown in Fig. 1. Values of γ and EFG variances, $\langle \mathbf{V}^2 \rangle$ [see Eq. (1)] are given in Table I, and \mathbf{V}_{CL} and \mathbf{V}_{QM} probability distributions are shown in Fig. S-2 of the supplementary material.

A linear relationship appears to hold between \mathbf{V}_{CL} and \mathbf{V}_{QM} for all simulated temperatures, and we find that γ increases from 11.1 at 298 K to 11.6 at 500 K. These values of γ are somewhat larger than seen in water ($\gamma_{\text{H}_2\text{O}} = 8.3\text{--}10.5$).³⁶ Because γ has been shown to be sensitive to the exact details of the force field and local solvent structure,³⁶ we refrain from interpreting this difference further, except to say that γ is not very different for Na⁺ in [Im₂₁][BF₄]

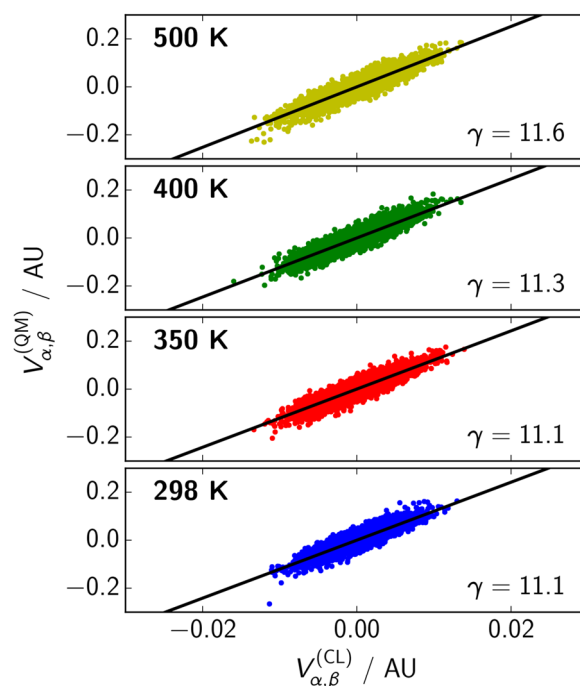


FIG. 1. Correlation plots of \mathbf{V}_{CL} and \mathbf{V}_{QM} (points), with fits to Eq. (5) (black line). The atomic units (AU) used for the EFG are those reported by the Q-Chem software, 1 AU = $9.717\,36 \times 10^{21}$ V m^{−2}.

TABLE I. Sternheimer anti-shielding coefficients, γ , and EFG variances for Na^+ in $[\text{Im}_{21}][\text{BF}_4]$ at each simulated temperature. These coefficients were determined by fitting the plots of \mathbf{V}_{CL} to \mathbf{V}_{QM} to Eq. (5), as shown in Fig. 1. Performing the Sternheimer analysis on five 200 point subsets of the data allows us to estimate a standard deviation of 1–2 % for γ and the variances.

T (K)	γ	$\langle \mathbf{V}_{\text{QM}}^2 \rangle (10^2 \text{ AU}^2)$	$\langle \mathbf{V}_{\text{CL}}^2 \rangle (10^2 \text{ AU}^2)$
500	11.6	2.40	2.05
400	11.3	2.00	1.66
350	11.1	1.88	1.57
298	11.1	1.67	1.34

than it is in water. After application of the Sternheimer correction to \mathbf{V}_{CL} , we find that both \mathbf{V}_{CL} and \mathbf{V}_{QM} are normally distributed (Fig. S-2), and that the variance of \mathbf{V}_{CL} is 15%–20% smaller than that of \mathbf{V}_{QM} — also a common observation for simulations in water.³⁶ These data show that the Sternheimer approximation is as valid in $[\text{Im}_{21}][\text{BF}_4]$ as it is in water.

B. EFG correlation functions

Now that we are confident in the static EFG properties of the $\text{Na}^+ / [\text{Im}_{21}][\text{BF}_4]$ system, we turn to the EFG dynamics through calculation of $C_{\text{EFG}}(t)$ [Eq. (2)]. Even though we have demonstrated that the Sternheimer approximation holds for the EFG variance, it is not a given that the frame-to-frame correlations will also hold. To ensure that $C_{\text{EFG}}(t)$ is independent of the method of EFG calculation, we took a 500 ps portion of the 500 K trajectory and evaluated the EFG at the Na^+ nucleus every 0.01 ps, using the QM and CL methods. Correlation functions were then calculated from each EFG evaluation method, and the resulting $C_{\text{EFG}}(t)$ is shown in the top panel of Fig. 2. Both evaluations of $C_{\text{EFG}}(t)$ are strongly bimodal, with ~95% of the decay occurring in the first 200 fs, followed by a slowly decaying tail. We will call the fast portion the “inertial” component of the decay, because motions on the sub-0.5 ps time scale are dominated by the inertia of the molecules, as they have not had time to collide with a neighbor. The tail will be referred to as the “diffusive” component, because motions on these longer timescales are expected to be controlled by the rotational and translational diffusion of solvent molecules around Na^+ .

The diffusive portion of $C_{\text{EFG}}(t)$ is effectively the same for the QM and CL evaluations, but the inertial dynamics for the QM $C_{\text{EFG}}(t)$ appear faster than that for CL. This is somewhat surprising, given that the EFG is evaluated from the exact same set of coordinates. We attribute this difference to the mobility of charge in the QM calculations, which is not possible in the CL calculation. When the QM calculation is performed, electrons in the QM region are allowed to move, in order to achieve self-consistency. This motion is not possible in the CL calculation, because the atomic point charges are fixed. Therefore, the QM calculation has an extra de-correlation pathway, not captured in the CL evaluation, and the resulting QM inertial dynamics are slightly faster than that of CL. On the diffusive timescale, these slight variations are not significant to the EFG magnitude, because the solvent nuclei have had time to substantially change position, overshadowing the effect of the slight changes in the frame-to-frame atomic charges. As we shall demonstrate, the

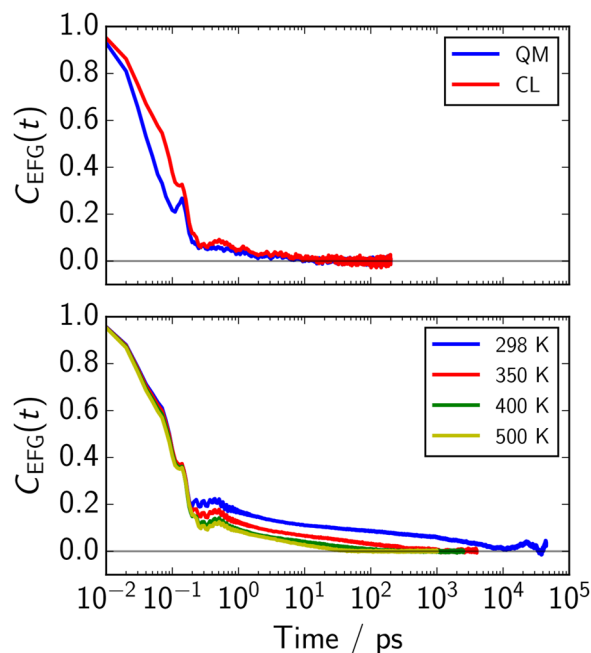


FIG. 2. Top: $C_{\text{EFG}}(t)$ calculated using either \mathbf{V}_{CL} or \mathbf{V}_{QM} from a 500 ps segment of the 500 K trajectory. Bottom: Temperature dependent $C_{\text{EFG}}(t)$ calculated from \mathbf{V}_{CL} .

integral EFG correlation time, $\langle \tau_{\text{EFG}} \rangle$, is dominated by the diffusive portion of $C_{\text{EFG}}(t)$; therefore, we are not concerned with the small difference in inertial dynamics and will use the CL evaluation of $C_{\text{EFG}}(t)$ for the rest of this work.

EFG correlation functions for each simulated temperature, calculated from \mathbf{V}_{CL} , are shown in the bottom panel of Fig. 2. Each temperature shows strongly bimodal decay, with small-amplitude oscillations that are visible until 2–3 ps. The oscillations of the EFG correlation functions, especially the pronounced bump at 100 fs, are correlated with the oscillations of the Na^+ velocity autocorrelation function (Fig. S-3). For calculation of $\langle \tau_{\text{EFG}} \rangle$, we fit the temperature-dependent correlation functions of Fig. 2 to the sum of an exponential and stretched exponential function according to

$$C_{\text{EFG}}(t) = h \left[a_1 e^{-t/\tau_1} + (1 - a_1) e^{-(t/\tau_2)^\beta} \right], \quad (8)$$

where h is the overall height and a_1 the amplitude of the exponential component. The β in Eq. (8) is termed the “stretching parameter” and has a range of $\beta = 0$ –1. A value of $\beta = 1$ corresponds to a single exponential, and smaller β values correspond to larger distributions of time constants and more broadly distributed dynamics. Integral times for Eq. (8) are calculated from

$$\langle \tau_{\text{EFG}} \rangle = a_1 \tau_1 + (1 - a_1) \langle \tau_{\text{str}} \rangle; \quad \langle \tau_{\text{str}} \rangle = \frac{\tau_2}{\beta} \Gamma(\beta^{-1}). \quad (9)$$

Fitting parameters for the temperature-dependent $C_{\text{EFG}}(t)$ are given in Table II. As is also evident from visual inspection, the fits show that the amplitude of the inertial component, a_1 , decreases with decreasing temperature, but its time constant, τ_1 , is insensitive

TABLE II. Parameters of fits of $C_{\text{EFG}}(t)$ to Eq. (8). Also included are viscosities from VFT fits to viscosities, calculated using the method of Zhang *et al.*⁶⁶ Calculations of $C_{\text{EFG}}(t)$ from consecutive 5 ns (500 K) or 10 ns (298 K) pieces of the trajectory allows us to calculate a standard deviation for $\langle\tau_{\text{EFG}}\rangle$ of 17% at 500 K and 77% at 298 K.

T (K)	h	a_1	τ_1 (ps)	τ_2 (ps)	β	$\langle\tau_{\text{str}}\rangle$ (ps)	$\langle\tau_{\text{EFG}}\rangle$ (ps)	T_1 (ms)	η (mPa s)
500	1.05	0.900	0.091	6.40	0.726	7.84	0.864	12.0	4.33
400	1.06	0.872	0.091	6.88	0.424	19.6	2.60	4.09	26.5
350	1.08	0.808	0.089	7.82	0.273	114	21.9	0.514	72.5
298	1.12	0.756	0.085	41.4	0.165	33 400	8130	0.001 56	248

to temperature. The diffusive component slows down considerably as temperature decreases, with a concomitant decrease in β , indicating that the dynamics become more heterogeneous as they become slower. We also observe relatively small values of β compared to what is usually encountered, indicating that the diffusive EFG dynamics in this system are especially heterogeneous. The large magnitude of $\langle\tau_{\text{str}}\rangle$ relative to τ_1 causes it to dominate $\langle\tau_{\text{EFG}}\rangle$, even if it only comprises 10%–25% of the decay. The slow dynamics of the diffusive component and correspondingly slow convergence of $C_{\text{EFG}}(t)$ at low temperature reinforce the utility of the Sternheimer approximation and classical MD for calculation of the EFG, in comparison to expensive quantum mechanical calculations.

Predicted T_1 times are also provided in Table II. These times are calculated according to Eq. (3) using $\langle V_{\text{CL}}^2 \rangle$ from Table I, $\langle\tau_{\text{EFG}}\rangle$ from Table II, and a nuclear quadrupole moment of $Q = 104$ mb for Na^+ .⁶⁷ Our simulations predict T_1 to range from 0.001 56 ms at 500 K to 12.0 ms at 298 K. These simulated T_1 times are expected to be faster than the experimental times, because the $[\text{Im}_{21}][\text{BF}_4]$ model used here is non-polarizable and fully charged (i.e., $[\text{Im}_{21}]^+$ and $[\text{BF}_4]^-$ have charges of $\pm 1e$). Partial charges and polarizability are known to speed up the dynamics of the system

and are commonly used to match simulated ionic liquid dynamics with experiments.⁶⁸ Due to the current lack of experimental data on this system, we will refrain from interpreting the T_1 times further.

In the analysis of diffusive processes, it is natural to compare integral times to predictions from molecular hydrodynamics. If the EFG dynamics behave hydrodynamically, $\langle\tau_{\text{EFG}}\rangle$ is expected to be proportional to the ratio of viscosity to temperature:

$$\langle\tau_{\text{EFG}}\rangle \propto (\eta T^{-1})^p; \quad p = 1, \quad (10)$$

where η is the viscosity. Deviations from $p = 1$ indicate the presence of molecular motions other than small-step diffusion in the dynamics. Values of τ_1 , τ_{str} , and $\langle\tau_{\text{EFG}}\rangle$ are plotted against ηT^{-1} in Fig. 3. Viscosities of the simulated ionic liquid were first determined using the method of Maginn *et al.*, then fit to the Vogel–Fulcher–Tammann (VFT) relation. The results of these calculations are given in Table II. These data show that the inertial times are insensitive to ηT^{-1} , which is expected, because inertial dynamics depend on the distribution of molecular velocities and not the medium's viscosity. On the other hand, $\langle\tau_{\text{EFG}}\rangle$ does not follow a power law (a straight line on the log-log plot) with respect to ηT^{-1} , indicating strongly non-hydrodynamic behavior. This observation suggests that the EFG dynamics are not controlled by one simple, small-step, diffusive motion, but may result from contributions of different types of molecular motions with different couplings to solvent viscosity. The origin of this pronounced non-hydrodynamic behavior and highly distributed dynamics will be the subject of the remainder of this work.

IV. DISCUSSION

A. Solvation shell structure

In order to understand which solvent motions are responsible for the heterogeneous and non-hydrodynamic EFG dynamics, we must first examine the local solvent environment around the Na^+ cation. Figure 4 shows radial distribution functions, $g(r)$, calculated between Na^+ and the $[\text{Im}_{21}]^+$ center-of-mass, the $[\text{BF}_4]^-$ center of mass, and all F atoms from $[\text{BF}_4]^-$. Coordination numbers for these species are provided in Table III and were calculated by integrating the associated number density to a specific distance r' :

$$N_i = 4\pi\rho \int_0^{r'} g_i(r)r^2 dr, \quad (11)$$

where ρ is the bulk number density of species i . At all temperatures, Na^+ is surrounded by 4 $[\text{BF}_4]^-$ anions, which are, in turn,

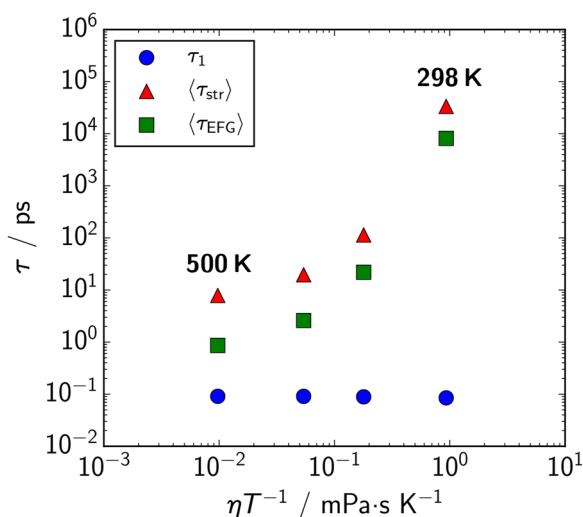


FIG. 3. Correlation times of $C_{\text{EFG}}(t)$ vs ηT^{-1} . Note that purely hydrodynamic behavior of these correlation times would be reflected by a linear dependence on ηT^{-1} with a slope of one [Eq. (10)].

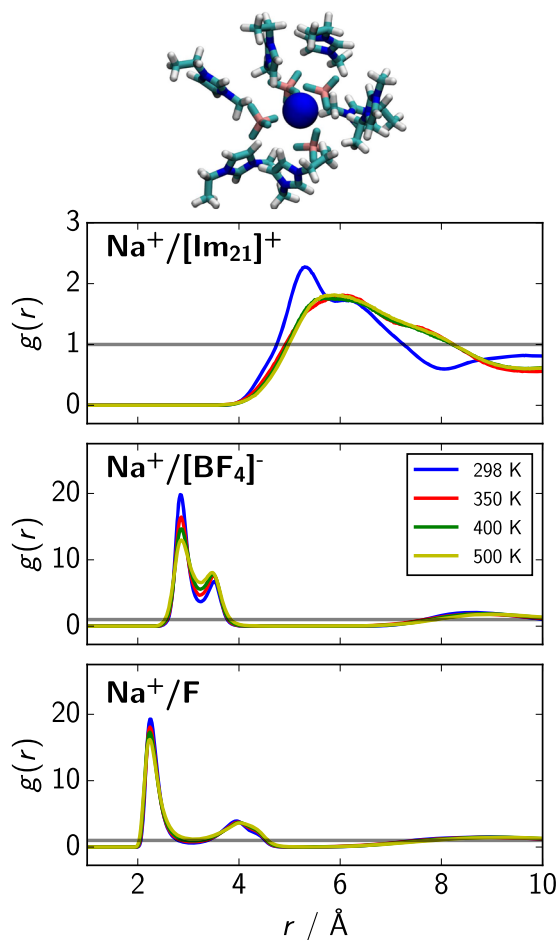


FIG. 4. Radial distribution functions, $g(r)$, for the distance between Na^+ and the center-of-mass of $[\text{Im}_{21}]^+$ (top), the center-of-mass of $[\text{BF}_4]^-$ (middle), and F atoms (bottom). A representative snapshot of solvent molecules in the vicinity of Na^+ at 350 K is shown at the top.

surrounded by a shell of $[\text{Im}_{21}]^+$ cations. By integration of the first peak in the $\text{Na}^+/\text{F}g(r)$, we find that Na^+ is directly coordinated by ~ 6 F atoms, whereas all 16 F atoms from the 4 $[\text{BF}_4]^-$ anions are found, if the integration is extended to 5.25 nm. It is noteworthy that these coordination numbers are insensitive to temperature, suggesting that the structure around Na^+ is similar for all simulated temperatures. This local solvent structure is illustrated by the representative snapshot at the top of Fig. 4. The $[\text{BF}_4]^-$ ions in the solvation shell are in a tetrahedral arrangement around the Na^+ . Calculations of tetrahedral structure parameters indicate a highly tetrahedral structure similar to that of hexagonal water ice (Fig. S-4).

Two peaks in the $\text{Na}^+/\text{F}g(r)$ are observed, which suggests that there are two primary $[\text{BF}_4]^-$ conformations in the solvation shell. The closer peak at 2.85 Å corresponds to $[\text{BF}_4]^-$ ions, with two F atoms coordinated to Na^+ . This configuration allows $[\text{BF}_4]^-$ to approach closer to Na^+ than singly-coordinated $[\text{BF}_4]^-$ anions, which appear at 3.50 Å. As temperature increases, the $\text{Na}^+/\text{F}g(r)$

TABLE III. The average coordination numbers were calculated by integrating number densities, $\rho(r) = 4\pi r^2 \rho g(r)$, to the limit specified in the header.

T (K)	$\langle N_{[\text{BF}_4]^-} \rangle_{r \leq 5.25 \text{ (Å)}}$	$\langle N_{\text{F}} \rangle_{r \leq 2.90 \text{ (Å)}}$	$\langle N_{\text{F}} \rangle_{r \leq 5.25 \text{ (Å)}}$
500	4.22	6.05	16.90
400	4.00	5.89	15.99
350	4.00	6.02	16.00
298	4.00	6.27	16.00

$g(r)$ broadens, while the doubly coordinated peak decreases, without a concomitant increase in the singly coordinated peak. This suggests that instead of exchanging doubly coordinated $[\text{BF}_4]^-$ for singly coordinated, more disorder is present in the solvation shell at higher temperatures. Because γ for monatomic ions in water was found to correlate with the hydrogen coordination number,^{28,36} we calculated γ for simulation frames with differing values of N_{F} . These results are plotted in Fig. 5 and tabulated in Table S-1. We find that γ is weakly correlated with N_{F} , which, in conjunction with the temperature dependent changes in $g(r)$, suggests that the slight temperature dependence of γ (Table I) may be related to subtle changes in the $[\text{BF}_4]^-$ configuration around Na^+ with changing temperature.

Not only is Na^+ solvated solely by $[\text{BF}_4]^-$ anions, but the exchange of $[\text{BF}_4]^-$ ions in-and-out of the solvation shell is remarkably slow. Representative trajectory segments of the Na^+/F separation distance at 298, 350, and 400 K are shown in Fig. 6, and full trajectories for every $[\text{BF}_4]^-$ that enters the solvation shell at all temperatures are shown in Fig. S-5. No $[\text{BF}_4]^-$ were observed to exit the solvation shell during the entire 50 ns trajectory at 298 K. Other $[\text{BF}_4]^-$ that are outside the solvation shell are substantially more mobile and diffuse throughout the simulation box (Fig. S-5). Exchanges are rare even at higher temperatures, examples

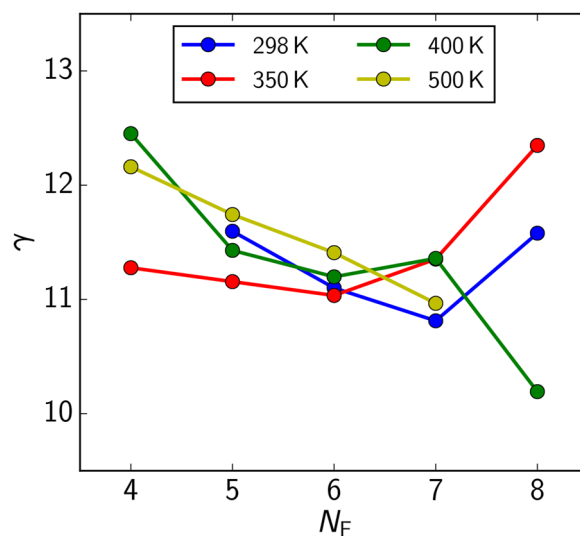


FIG. 5. Sternheimer coefficients for Na^+ with different fluorine coordination numbers, N_{F} .

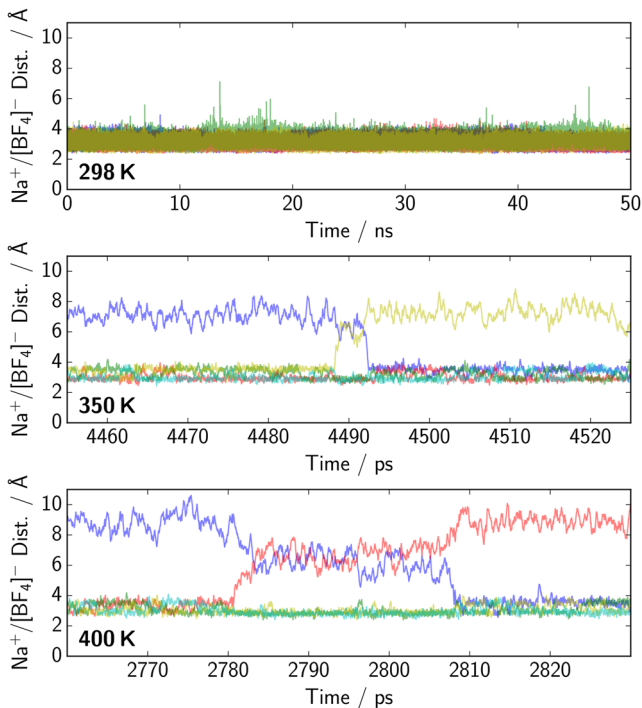


FIG. 6. Representative trajectories of the $\text{Na}^+/\text{[BF}_4\text{]}^-$ separation distance. Each color represents a different $[\text{BF}_4]^-$ anion. Four anions are shown in the top panel, and five are shown in the middle and bottom. Note that the vertical scale is the same for all plots, and the middle and bottom both show a 70 ps time window.

of which are shown in the bottom two panels of Fig. 6. Only 1 and 4 of these events were observed in 25 ns at 350 and 400 K, respectively. Exchange of solvation shell $[\text{BF}_4]^-$ anions also does not appear to be diffusive, but proceeds through the formation of a transition state, where one $[\text{BF}_4]^-$ ‘jumps’ out of the solvation shell, causing the remaining three $[\text{BF}_4]^-$ to contract. An external $[\text{BF}_4]^-$ then has a chance to enter the solvation shell, and the four $[\text{BF}_4]^-$ arrangement is recovered. The rarity of these events and the short time spent in the transition state indicate that ion exchange events cannot be the

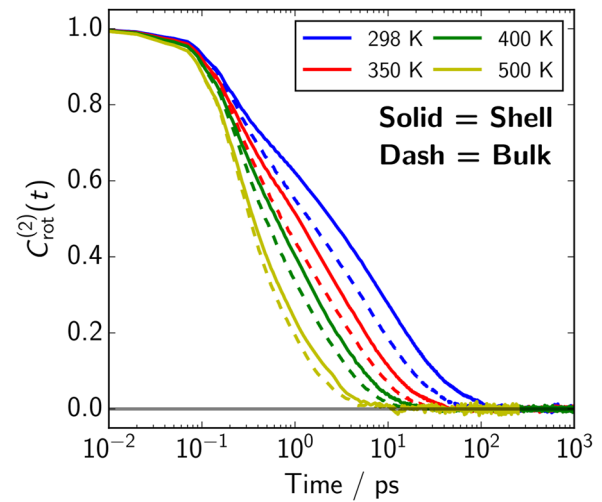


FIG. 7. Temperature-dependent $C_{\text{rot}}^{(2)}(t)$ for $[\text{BF}_4]^-$ molecules inside (“Shell”) and outside (“Bulk”) the Na^+ solvation shell.

primary source of the strongly heterogeneous EFG dynamics seen in Fig. 2, nor for the non-hydrodynamic behavior in Fig. 3.

B. Dynamics of the solvation shell

Because of the persistence of the $[\text{BF}_4]^-$ anions around Na^+ , we postulate that the EFG dynamics must be primarily due to rotation and translation of the solvent-shell $[\text{BF}_4]^-$ anions around Na^+ . Rotations of $[\text{BF}_4]^-$ anions will randomize the position of the F atoms around Na^+ , as the $[\text{BF}_4]^-$ anions slowly translate about Na^+ . We will investigate the rotational dynamics of $[\text{BF}_4]^-$ using the second-rank rotational time correlation function

$$C_{\text{rot}}^{(2)}(t) = \frac{3}{2} \langle \hat{u}(0) \cdot \hat{u}(t) \rangle - \frac{1}{2}, \quad (12)$$

where $\hat{u}(t)$ is a unit vector lying along the B–F bond in a $[\text{BF}_4]^-$ anion at time t . This function describes the randomization of the orientation of a $[\text{BF}_4]^-$ anion as it diffuses. We choose $C_{\text{rot}}^{(2)}(t)$ instead of the first-rank correlation function, because it can be measured by

TABLE IV. Parameters of fits of $C_{\text{rot}}^{(2)}(t)$ to Eq. (8). Rows labeled “Shell” refer to $[\text{BF}_4]^-$ anions in the solvation shell, and “Bulk” for anions outside of it.

T (K)	Location	h	a_1	τ_1 (ps)	τ_2 (ps)	β	$\langle \tau_{\text{str}} \rangle$ (ps)	$\langle \tau_{\text{rot}} \rangle$ (ps)
500 K	Shell	1.05	0.743	0.376	2.20	1.000	2.20	0.85
	Bulk	1.05	0.839	0.395	2.23	1.000	2.23	0.69
400 K	Shell	1.03	0.519	0.387	3.26	0.910	3.41	1.84
	Bulk	1.04	0.630	0.395	3.00	1.000	3.00	1.36
350 K	Shell	1.03	0.351	0.354	4.52	0.735	5.47	3.68
	Bulk	1.03	0.505	0.391	4.43	0.888	4.69	2.52
298 K	Shell	1.03	0.246	0.325	9.51	0.602	14.2	10.8
	Bulk	1.03	0.350	0.376	7.09	0.699	8.98	5.97

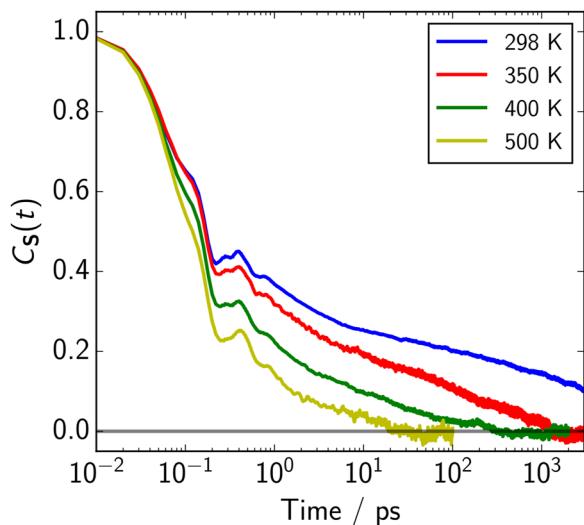


FIG. 8. Correlation functions of solvent shell center-of-mass fluctuations.

other T_1 relaxation measurements.¹² Because the rotational dynamics of $[\text{BF}_4]^-$ in the solvation shell may be different than in the bulk, we calculated $C_{\text{rot}}^{(2)}(t)$ separately for ions inside and outside the solvation shell. The results of these calculations are shown in Fig. 7, and parameters from fits of $C_{\text{rot}}^{(2)}(t)$ to Eq. (8) are provided in Table IV.

Rotations of $[\text{BF}_4]^-$ are slower in the solvation shell than in the bulk, likely due to the strong coordination with the charge-dense Na^+ ion. The difference between the bulk and shell dynamics changes with temperature, with $[\text{BF}_4]^-$ rotations being 23% slower in the solvation shell at 500 K compared to being 80% slower at 298 K. Rotations in the solvation shell are also more heterogeneous, given the slightly smaller values of β , and at all locations and temperatures, β is significantly larger than that seen in $C_{\text{EFG}}(t)$. At high temperatures, the heterogeneity disappears, and $\beta \rightarrow 1$. Even though $\langle \tau_{\text{rot}} \rangle$ is roughly the same as $\langle \tau_{\text{EFG}} \rangle$ at 500 K, it is ~ 3 orders of magnitude smaller than $\langle \tau_{\text{EFG}} \rangle$ at 298 K. Note that this is the opposite of what is observed in water, where water rotations are slower than the EFG dynamics at the Na^+ nucleus.^{24,32} It is clear from these data that the EFG dynamics are not completely controlled by $[\text{BF}_4]^-$ rotations, and we must find some other description of solvent motion that contributes to the EFG de-correlation.

Traditional descriptions of translational motion, such as mean-squared displacements and diffusion coefficients, are not useful here, because the solvation shell $[\text{BF}_4]^-$ anions are essentially

bound to Na^+ and do not freely diffuse. Additionally, translational motions of single molecules do not lend themselves well to correlation functions, because they do not have a well-defined limiting value as $t \rightarrow \infty$. These factors, in addition to the collective nature of the EFG, lead us to seek a collective positional variable, to describe translations of the $[\text{BF}_4]^-$ ions around Na^+ . We chose to use the fluctuations of the solvation shell center-of-geometry, described by^{31,32}

$$\mathbf{S} = \sum_{i \in \text{S}} \mathbf{r}_i, \quad (13)$$

where \mathbf{r}_i is the position of the B in $[\text{BF}_4]^-$ relative to Na^+ , and the sum runs over all four $[\text{BF}_4]^-$ anions in the solvation shell. The three components of \mathbf{S} are then used to determine correlation functions:

$$C_S(t) = \frac{1}{\sum_{\alpha} S_{\alpha}^2(0)} \left\langle \sum_{\alpha} S_{\alpha}(0) S_{\alpha}(t) \right\rangle, \quad (14)$$

where α refers to the three Cartesian axes. Correlation functions for \mathbf{S} are shown in Fig. 8, and parameters from fits to Eq. (8) are given in Table V.

As has been observed for water,^{31,32} $C_S(t)$ shows bi-modal dynamics roughly similar to that of $C_{\text{EFG}}(t)$, with a prominent inertial component and long diffusive tail. Integral times for $C_S(t)$ are the same as $C_{\text{EFG}}(t)$ at 500 K, but are slower than $C_{\text{EFG}}(t)$ for all other temperatures. Values of β are quite small and comparable to those found for $C_{\text{EFG}}(t)$. As with $[\text{BF}_4]^-$ rotations, it appears that translational motions cannot fully account for the EFG dynamics. Figure 9 shows correlation times for $C_{\text{EFG}}(t)$, $C_{\text{rot}}^{(2)}(t)$, and $C_S(t)$ plotted vs ηT^{-1} . These data show that all three correlation times converge at 500 K, but for all lower temperatures, $\langle \tau_{\text{EFG}} \rangle$ is intermediate between $\langle \tau_{\text{rot}} \rangle$ and $\langle \tau_S \rangle$, being closer to $\langle \tau_{\text{rot}} \rangle$ at 350 K and closer to $\langle \tau_S \rangle$ at 298 K.

The non-hydrodynamic behavior observed in $\langle \tau_{\text{EFG}} \rangle$ can thus be explained by the different relationship to viscosity for solvent rotations and translations. The EFG is influenced by a mixture of rotational and translational motions of $[\text{BF}_4]^-$ in the solvation shell, and since these motions are coupled differently to the bulk viscosity, the EFG has a non-hydrodynamic ηT^{-1} dependence. At lower temperatures, the rotations are extremely fast compared to translations, which randomizes the F atom EFG contribution quickly, but has no effect on the $+0.96e$ charge carried by the B. Therefore, the primary mechanism for EFG de-correlation at low temperature/high viscosity is through $[\text{BF}_4]^-$ translations, causing $\langle \tau_{\text{EFG}} \rangle$ to approach $\langle \tau_S \rangle$. As temperature increases, the fast rotations and faster translations de-correlate $C_{\text{EFG}}(t)$ more quickly, and $\langle \tau_{\text{EFG}} \rangle$ begins to approach $\langle \tau_{\text{rot}} \rangle$. Finally, at the highest temperatures, rotational and

TABLE V. Parameters of fits of $C_S(t)$ to Eq. (8).

T (K)	h	a_1	τ_1 (ps)	τ_2 (ps)	β	$\langle \tau_{\text{str}} \rangle$ (ps)	$\langle \tau_S \rangle$ (ps)
500	1.11	0.743	0.101	1.95	0.558	3.25	0.910
400	1.14	0.610	0.107	2.92	0.326	19.0	7.47
350	1.15	0.528	0.110	10.8	0.248	273	129
298	1.16	0.516	0.109	77.5	0.172	40 000	19 400

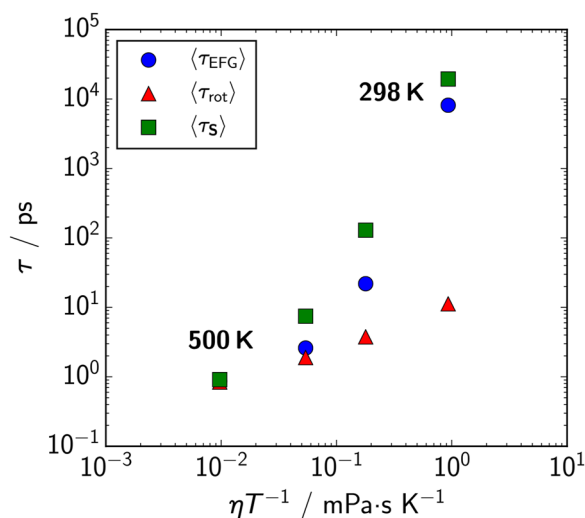


FIG. 9. Integral times of $C_{\text{EFG}}(t)$, $C_{\text{rot}}^{(2)}(t)$ for solvation shell $[\text{BF}_4]^-$, and $C_{\text{S}}(t)$ vs ηT^{-1} .

translational motions happen on the same timescale, and $\langle\tau_{\text{EFG}}\rangle$, $\langle\tau_{\text{rot}}\rangle$, and $\langle\tau_{\text{S}}\rangle$ become essentially the same. These results lead us to conclude that solvent rotations and translations, both influence the EFG dynamics, but their relative contributions vary, depending on the viscosity, leading to the observed non-hydrodynamic dependence of $\langle\tau_{\text{EFG}}\rangle$ on ηT^{-1} .

V. CONCLUSIONS

The results of our simulations have established a framework for studying EFG fluctuations at monatomic ion nuclei in ionic liquids. We have demonstrated that the Sternheimer approximation can be applied to this prototypical solute ion/ionic liquid pair and that the Sternheimer anti-shielding coefficients are similar to those found for water. After applying the Sternheimer correction, EFG variances for the classical EFG evaluation are $\sim 20\%$ smaller than those for the full QM evaluation, again similar to analogous calculations conducted in water. Additionally, EFG correlation functions calculated using CL and QM EFGs are interchangeable, apart from the slightly faster inertial dynamics in the QM data. Based on these observations, we are able to confidently use the computationally inexpensive CL EFG for further study of the EFG dynamics in $\text{Na}^+/\text{[Im}_{21}\text{]BF}_4$.

The $C_{\text{EFG}}(t)$ for at all temperatures exhibits strongly bimodal dynamics, with a prominent sub-picosecond inertial component accounting for 75%–90% of the de-correlation and the rest attributable to a long diffusive tail with highly distributed dynamics. Integral times of $C_{\text{EFG}}(t)$ exhibited a non-linear dependence on ηT^{-1} , suggesting strongly non-hydrodynamic behavior. The origin of this behavior was examined by investigating the local solvent dynamics around the Na^+ ion. The solvation shell around Na^+ in $[\text{Im}_{21}][\text{BF}_4]$ at all temperatures consists of four $[\text{BF}_4]^-$ anions in a tetrahedral arrangement. These solvation shell $[\text{BF}_4]^-$ rarely exchange on the 25–50 ns timescale of the simulations, indicating that the EFG fluctuations will be primarily controlled by rotations

and translations of $[\text{BF}_4]^-$ in the Na^+ solvation shell. Analysis of the solvent shell $[\text{BF}_4]^-$ rotational and translational dynamics through $C_{\text{rot}}^{(2)}(t)$ and $C_{\text{S}}(t)$ showed that $\langle\tau_{\text{EFG}}\rangle$ is intermediate between $\langle\tau_{\text{rot}}\rangle$ and $\langle\tau_{\text{S}}\rangle$, which have different couplings to ηT^{-1} . We conclude that the subtle interplay between translations and rotations of solvent shell $[\text{BF}_4]^-$, and their different viscosity couplings, are what determine $\langle\tau_{\text{EFG}}\rangle$ and its coupling to viscosity.

These initial simulations on a single ion/ionic liquid pair demonstrate a need for further experimental and computational study. Temperature dependent T_1 measurements are needed to experimentally confirm the non-hydrodynamic dynamics predicted by these simulations. The $[\text{Im}_{21}][\text{BF}_4]$ solvent chosen here is somewhat special, in that its rotations are weakly coupled to viscosity, due to the quasi-spherical shape and small rotational volume of $[\text{BF}_4]^-$. Simulations and experiments on ionic liquids with different anions would be expected to exhibit different ηT^{-1} coupling, due to differences in anion shape and symmetry. Additionally, solute ions of different sizes are expected to perturb the lattice structure of the solvent ionic liquids differently, potentially leading to solute-dependent dynamics. Negatively charged solutes may also exhibit starkly different dynamics than positively charged solutes, as they would be expected to be solvated primarily by IL cations. The T_1 measurement, when combined with simulations, can be a powerful tool for disentangling the contributions of different solvent motions to solute and solvent dynamics and probing the local solvent environment.

SUPPLEMENTARY MATERIAL

System-size dependent classical EFG probability distributions, V_{CL} and V_{QM} probability distributions, Na^+ velocity autocorrelation functions at 500 K, details on the tetrahedral parameter calculations, tables of coordination-number dependent γ , and full $[\text{BF}_4]^-/\text{Na}^+$ separation trajectories at all temperatures can be found in the [supplementary material](#).

ACKNOWLEDGMENTS

C.A.R. would like to thank Mark Maroncelli, Sourav Palchowdhury, and Kallol Mukherjee for insightful conversations. M.K. would like to acknowledge funding from ERC Grant No. 640645, B.K. from the German Funding Agency (Grant No. 441102113), and K.D.-K. from the Wolfgang Gentner Program of the German Federal Ministry of Education and Research (Grant No. 05E15CHA). All quantum chemical calculations were performed on the Yggdrasil cluster at Université de Genève.

AUTHOR DECLARATIONS

Conflict of Interest

The authors have no conflicts to disclose.

Author Contributions

Yann Gimbal-Zofka: Formal analysis (supporting); Investigation (supporting); Writing – review & editing (equal). **Beatrice Karg:**

Conceptualization (equal); Investigation (supporting); Methodology (supporting); Writing – review & editing (supporting); **Katarzyna Dziubinska-Kühn**: Conceptualization (supporting); Methodology (equal); Writing – review & editing (supporting). **Magdalena Kowalska**: Conceptualization (equal); Funding acquisition (equal); Writing – review & editing (supporting). **Tomasz A. Wesolowski**: Conceptualization (equal); Data curation (lead); Formal analysis (lead); Investigation (lead); Methodology (equal); Visualization (lead); Writing – original draft (lead); Writing – review & editing (supporting). **Christopher A. Rumble**: Conceptualization (supporting); Data curation (lead); Formal analysis (lead); Investigation (lead); Methodology (lead); Visualization (lead); Writing – original draft (lead); Writing – review & editing (lead).

DATA AVAILABILITY

The data that support the findings of this study are available from the corresponding author upon reasonable request.

REFERENCES

- 1 E. W. Castner, C. J. Margulis, M. Maroncelli, and J. F. Wishart, "Ionic liquids: Structure and photochemical reactions," *Annu. Rev. Phys. Chem.* **62**, 85–105 (2011).
- 2 J. P. Hallett and T. Welton, "Room-temperature ionic liquids: Solvents for synthesis and catalysis. 2," *Chem. Rev.* **111**, 3508–3576 (2011).
- 3 D. R. MacFarlane, N. Tachikawa, M. Forsyth, J. M. Pringle, P. C. Howlett, G. D. Elliott, J. H. Davis, M. Watanabe, P. Simon, and C. A. Angell, "Energy applications of ionic liquids," *Energy Environ. Sci.* **7**, 232–250 (2013).
- 4 R. Hayes, G. G. Warr, and R. Atkin, "Structure and nanostructure in ionic liquids," *Chem. Rev.* **115**, 6357–6426 (2015).
- 5 G. A. Giffin, "Ionic liquid-based electrolytes for 'beyond lithium' battery technologies," *J. Mater. Chem. A* **4**, 13378–13389 (2016).
- 6 A. A. C. Toledo Hijo, G. J. Maximo, M. C. Costa, E. A. C. Batista, and A. J. A. Meirelles, "Applications of ionic liquids in the food and bioproducts industries," *ACS Sustainable Chem. Eng.* **4**, 5347–5369 (2016).
- 7 M. Watanabe, M. L. Thomas, S. Zhang, K. Ueno, T. Yasuda, and K. Dokko, "Application of ionic liquids to energy storage and conversion materials and devices," *Chem. Rev.* **117**, 7190–7239 (2017).
- 8 T. Welton, "Ionic liquids: A brief history," *Biophys. Rev.* **10**, 691–706 (2018).
- 9 Y.-L. Wang, B. Li, S. Sarman, F. Mocci, Z.-Y. Lu, J. Yuan, A. Laaksonen, and M. D. Fayer, "Microstructural and dynamical heterogeneities in ionic liquids," *Chem. Rev.* **120**, 5798–5877 (2020).
- 10 A. J. Greer, J. Jacquemin, and C. Hardacre, "Industrial applications of ionic liquids," *Molecules* **25**, 5207 (2020).
- 11 R. Nanda and K. Damodaran, "A review of NMR methods used in the study of the structure and dynamics of ionic liquids," *Magn. Reson. Chem.* **56**, 62–72 (2018).
- 12 M. H. Levitt, *Spin Dynamics*, 2nd ed. (John Wiley & Sons, Ltd., 2008).
- 13 J. H. Antony, D. Mertens, A. Dölle, P. Wasserscheid, and W. R. Carper, "Molecular reorientational dynamics of the neat ionic liquid 1-butyl-3-methylimidazolium hexafluorophosphate by measurement of ^{13}C nuclear magnetic relaxation data," *ChemPhysChem* **4**, 588–594 (2003).
- 14 N. E. Heimer, J. S. Wilkes, P. G. Wahlbeck, and W. R. Carper, " ^{13}C NMR relaxation rates in the ionic liquid 1-ethyl-3-methylimidazolium butanesulfonate," *J. Phys. Chem. A* **110**, 868–874 (2006).
- 15 A. Wulf, R. Ludwig, P. Saisanker, and H. Weingärtner, "Molecular reorientation in ionic liquids: A comparative dielectric and magnetic relaxation study," *Chem. Phys. Lett.* **439**, 323–326 (2007).
- 16 K. Hayamizu, S. Tsuzuki, and S. Seki, "Molecular motions and ion diffusions of the room-temperature ionic liquid 1,2-dimethyl-3-propylimidazolium bis(trifluoromethylsulfonyl)amide (DMPImTfSA) studied by ^1H , ^{13}C , and ^{19}F NMR," *J. Phys. Chem. A* **112**, 12027–12036 (2008).
- 17 T. M. Alam, D. R. Dreyer, C. W. Bielawski, and R. S. Ruoff, "Combined measurement of translational and rotational diffusion in quaternary acyclic ammonium and cyclic pyrrolidinium ionic liquids," *J. Phys. Chem. B* **117**, 1967–1977 (2013).
- 18 C. A. Rumble, A. Kaintz, S. K. Yadav, B. Conway, J. C. Araque, G. A. Baker, C. Margulis, and M. Maroncelli, "Rotational dynamics in ionic liquids from NMR relaxation experiments and simulations: Benzene and 1-ethyl-3-methylimidazolium," *J. Phys. Chem. B* **120**, 9450–9467 (2016).
- 19 C. A. Rumble, C. Uitvlugt, B. Conway, and M. Maroncelli, "Solute rotation in ionic liquids: Size, shape, and electrostatic effects," *J. Phys. Chem. B* **121**, 5094–5109 (2017).
- 20 K. Dziubinska-Kühn, J. Croese, M. Pupier, J. Matysik, J. Viger-Gravel, B. Karg, and M. Kowalska, "Structural analysis of water in ionic liquid domains—A low pressure study," *J. Mol. Liq.* **334**, 116447 (2021).
- 21 V. Overbeck, H. Schröder, A.-M. Bonsa, K. Neymeyr, and R. Ludwig, "Insights into the translational and rotational dynamics of cations and anions in protic ionic liquids by means of NMR fast-field-cycling relaxometry," *Phys. Chem. Chem. Phys.* **23**, 2663–2675 (2021).
- 22 A. E. Khudozhitkov, P. Stange, A. G. Stepanov, D. I. Kolokolov, and R. Ludwig, "Structure, hydrogen bond dynamics and phase transition in a model ionic liquid electrolyte," *Phys. Chem. Chem. Phys.* **24**, 6064–6071 (2022).
- 23 S. Engström, B. Jönsson, and B. Jönsson, "A molecular approach to quadrupole relaxation. Monte Carlo simulations of dilute Li^+ , Na^+ , and Cl^- aqueous solutions," *J. Magn. Reson.* **50**, 1–20 (1982).
- 24 S. Engström, B. Jönsson, and R. W. Impey, "Molecular dynamic simulation of quadrupole relaxation of atomic ions in aqueous solution," *J. Chem. Phys.* **80**, 5481–5486 (1984).
- 25 J. E. Roberts and J. Schnitker, "Ionic quadrupolar relaxation in aqueous solution: Dynamics of the hydration sphere," *J. Phys. Chem.* **97**, 5410–5417 (1993).
- 26 M. Odelius and J. Kowalewski, "Molecular dynamics simulation of nuclear spin relaxation of $^7\text{Li}^+$ in water," *J. Chem. Soc., Faraday Trans.* **91**, 215–222 (1995).
- 27 P.-L. Chau and A. J. Hardwick, "A new order parameter for tetrahedral configurations," *Mol. Phys.* **93**, 511–518 (1998).
- 28 K. Aidas, H. Ågren, J. Kongsted, A. Laaksonen, and F. Mocci, "A quantum mechanics/molecular dynamics study of electric field gradient fluctuations in the liquid phase. The case of Na^+ in aqueous solution," *Phys. Chem. Chem. Phys.* **15**, 1621–1631 (2013).
- 29 S. Badu, L. Truflandier, and J. Autschbach, "Quadrupolar NMR spin relaxation calculated using ab initio molecular dynamics: Group 1 and group 17 ions in aqueous solution," *J. Chem. Theory Comput.* **9**, 4074–4086 (2013).
- 30 A. Carof, M. Salanne, T. Charpentier, and B. Rotenberg, "Accurate quadrupolar NMR relaxation rates of aqueous cations from classical molecular dynamics," *J. Phys. Chem. B* **118**, 13252–13257 (2014).
- 31 A. Carof, M. Salanne, T. Charpentier, and B. Rotenberg, "On the microscopic fluctuations driving the NMR relaxation of quadrupolar ions in water," *J. Chem. Phys.* **143**, 194504 (2015).
- 32 A. Carof, M. Salanne, T. Charpentier, and B. Rotenberg, "Collective water dynamics in the first solvation shell drive the NMR relaxation of aqueous quadrupolar cations," *J. Chem. Phys.* **145**, 124508 (2016).
- 33 A. Philips, A. Marchenko, L. A. Truflandier, and J. Autschbach, "Quadrupolar NMR relaxation from ab initio molecular dynamics: Improved sampling and cluster models versus periodic calculations," *J. Chem. Theory Comput.* **13**, 4397–4409 (2017).
- 34 A. Philips and J. Autschbach, "Quadrupolar NMR relaxation of Aqueous $^{127}\text{I}^-$, ^{131}Xe , and $^{133}\text{Cs}^+$: A first-principles approach from dynamics to properties," *J. Chem. Theory Comput.* **16**, 5835–5844 (2020).
- 35 M. Mohammadi, S. Benders, and A. Jerschow, "Nuclear magnetic resonance spin-lattice relaxation of lithium ions in aqueous solution by NMR and molecular dynamics," *J. Chem. Phys.* **153**, 184502 (2020).
- 36 I. Chubak, L. Scalfi, A. Carof, and B. Rotenberg, "NMR relaxation rates of quadrupolar aqueous ions from classical molecular dynamics using force-field specific Sternheimer factors," *J. Chem. Theory Comput.* **17**, 6006–6017 (2021).
- 37 D. Monti, E. Jönsson, M. R. Palacín, and P. Johansson, "Ionic liquid based electrolytes for sodium-ion batteries: Na^+ solvation and ionic conductivity," *J. Power Sources* **245**, 630–636 (2014).

- ³⁸J. M. Vicent-Luna, J. M. Ortiz-Roldan, S. Hamad, R. Tena-Zaera, S. Calero, and J. A. Anta, "Quantum and classical molecular dynamics of ionic liquid electrolytes for Na/Li-based batteries: Molecular origins of the conductivity behavior," *ChemPhysChem* **17**, 2473–2481 (2016).
- ³⁹P. Kubisiak and A. Eilmes, "Molecular dynamics simulations of ionic liquid based electrolytes for Na-ion batteries: Effects of force field," *J. Phys. Chem. B* **121**, 9957–9968 (2017).
- ⁴⁰M. Okoshi, C.-P. Chou, and H. Nakai, "Theoretical analysis of carrier ion diffusion in superconcentrated electrolyte solutions for sodium-ion batteries," *J. Phys. Chem. B* **122**, 2600–2609 (2018).
- ⁴¹F. Chen, P. Howlett, and M. Forsyth, "Na-ion solvation and high transference number in superconcentrated ionic liquid electrolytes: A theoretical approach," *J. Phys. Chem. C* **122**, 105–114 (2018).
- ⁴²L. Hakim, Y. Ishii, K. Matsumoto, R. Hagiwara, K. Ohara, Y. Umabayashi, and N. Matubayasi, "Transport properties of ionic liquid and sodium salt mixtures for sodium-ion battery electrolytes from molecular dynamics simulation with a self-consistent atomic charge determination," *J. Phys. Chem. B* **124**, 7291–7305 (2020).
- ⁴³K. Hayamizu, S. Tsuzuki, S. Seki, Y. Ohno, H. Miyashiro, and Y. Kobayashi, "Quaternary ammonium room-temperature ionic liquid including an oxygen atom in side chain/lithium salt binary electrolytes: Ionic conductivity and ^1H , ^7Li , and ^{19}F NMR studies on diffusion coefficients and local motions," *J. Phys. Chem. B* **112**, 1189–1197 (2008).
- ⁴⁴K. Hayamizu, S. Tsuzuki, S. Seki, K. Fujii, M. Suenaga, and Y. Umabayashi, "Studies on the translational and rotational motions of ionic liquids composed of *N*-methyl-*N*-propyl-pyrrolidinium (P13) cation and bis(trifluoromethanesulfonyl)amide and bis(fluorosulfonyl)amide anions and their binary systems including lithium salts," *J. Chem. Phys.* **133**, 194505 (2010).
- ⁴⁵K. Hayamizu, S. Tsuzuki, S. Seki, and Y. Umabayashi, "Nuclear magnetic resonance studies on the rotational and translational motions of ionic liquids composed of 1-ethyl-3-methylimidazolium cation and bis(trifluoromethanesulfonyl)amide and bis(fluorosulfonyl)amide anions and their binary systems including lithium salts," *J. Chem. Phys.* **135**, 084505 (2011).
- ⁴⁶T. Umecky, T. Takamuku, T. Matsumoto, E. Kawai, M. Takagi, and T. Funazukuri, "Effects of dissolved water on Li^+ solvation in 1-ethyl-3-methylimidazolium bis(trifluoromethanesulfonyl)amide ionic liquid studied by NMR," *J. Phys. Chem. B* **117**, 16219–16226 (2013).
- ⁴⁷A. Abragam, *The Principles of Nuclear Magnetism* (Oxford University Press, 1961).
- ⁴⁸R. Sternheimer, "On nuclear quadrupole moments," *Phys. Rev.* **80**, 102–103 (1950).
- ⁴⁹H. M. Foley, R. M. Sternheimer, and D. Tycko, "Nuclear quadrupole coupling in polar molecules," *Phys. Rev.* **93**, 734–742 (1954).
- ⁵⁰R. M. Sternheimer, "Shielding and antishielding effects for various ions and atomic systems," *Phys. Rev.* **146**, 140–160 (1966).
- ⁵¹R. M. Sternheimer, "Quadrupole antishielding factors of ions," *Phys. Rev.* **159**, 266–272 (1967).
- ⁵²R. M. Sternheimer, "Quadrupole shielding and antishielding factors for several atomic ground states," *Phys. Rev. A* **6**, 1702–1709 (1972).
- ⁵³P. W. Fowler, P. Lazzeretti, E. Steiner, and R. Zanasi, "The theory of Sternheimer shielding in molecules in external fields," *Chem. Phys.* **133**, 221–235 (1989).
- ⁵⁴M. J. Abraham, T. Murtola, R. Schulz, S. Páll, J. C. Smith, B. Hess, and E. Lindahl, "GROMACS: High performance molecular simulations through multi-level parallelism from laptops to supercomputers," *SoftwareX* **1–2**, 19–25 (2015).
- ⁵⁵J. N. Canongia Lopes, J. Deschamps, and A. A. H. Pádua, "Modeling ionic liquids using a systematic all-atom force field," *J. Phys. Chem. B* **108**, 2038–2047 (2004).
- ⁵⁶J. N. Canongia Lopes and A. A. H. Pádua, "Molecular force field for ionic liquids III: Imidazolium, pyridinium, and phosphonium cations; chloride, bromide, and dicyanamide anions," *J. Phys. Chem. B* **110**, 19586–19592 (2006).
- ⁵⁷L. Martínez, R. Andrade, E. G. Birgin, and J. M. Martínez, "PACKMOL: A package for building initial configurations for molecular dynamics simulations," *J. Comput. Chem.* **30**, 2157–2164 (2009).
- ⁵⁸This software can be found at <https://doi.org/10.5281/zenodo.4701065>.
- ⁵⁹U. Essmann, L. Perera, M. L. Berkowitz, T. Darden, H. Lee, and L. G. Pedersen, "A smooth particle mesh Ewald method," *J. Chem. Phys.* **103**, 8577–8593 (1995).
- ⁶⁰B. Hess, "P-LINCS: A parallel linear constraint solver for molecular simulation," *J. Chem. Theory Comput.* **4**, 116–122 (2008).
- ⁶¹G. Bussi, D. Donadio, and M. Parrinello, "Canonical sampling through velocity rescaling," *J. Chem. Phys.* **126**, 014101 (2007).
- ⁶²E. Epifanovsky, A. T. B. Gilbert, X. Feng, J. Lee, Y. Mao, N. Mardirossian, P. Pokhilko, A. F. White, M. P. Coons, A. L. Dempwolff, Z. Gan, D. Hait, P. R. Horn, L. D. Jacobson, I. Kaliman, J. Kusmann, A. W. Lange, K. U. Lao, D. S. Levine, J. Liu, S. C. McKenzie, A. F. Morrison, K. D. Nanda, F. Plasser, D. R. Rehn, M. L. Vidal, Z.-Q. You, Y. Zhu, B. Alam, B. J. Albrecht, A. Aldossary, E. Alguire, J. H. Andersen, V. Athavale, D. Barton, K. Begam, A. Behn, N. Bellonzi, Y. A. Bernard, E. J. Berquist, H. G. A. Burton, A. Carreras, K. Carter-Fenk, R. Chakraborty, A. D. Chien, K. D. Closser, V. Cofer-Shabica, S. Dasgupta, M. de Wergifosse, J. Deng, M. Diedenhofen, H. Do, S. Ehlert, P.-T. Fang, S. Fatehi, Q. Feng, T. Friedhoff, J. Gayvert, Q. Ge, G. Gidofalvi, M. Goldej, J. Gomes, C. E. González-Espinoza, S. Gulania, A. O. Gunina, M. W. D. Hanson-Heine, P. H. P. Harbach, A. Hauser, M. F. Herbst, M. Hernández Vera, M. Hodecker, Z. C. Holden, S. Houck, X. Huang, K. Hui, B. C. Huynh, M. Ivanov, Á. Jász, H. Ji, H. Jiang, B. Kaduk, S. Kähler, K. Khistyayev, J. Kim, G. Kis, P. Klunzinger, Z. Koczor-Benda, J. H. Koh, D. Kosenkov, L. Koulias, T. Kowalczyk, C. M. Krauter, K. Kue, A. Kunitsa, T. Kus, I. Ladžánszki, A. Landau, K. V. Lawler, D. Lefrançois, S. Lehtola, R. R. Li, Y.-P. Li, J. Liang, M. Lieenthal, H.-H. Lin, Y.-S. Lin, F. Liu, K.-Y. Liu, M. Loipersberger, A. Luenser, A. Manjanath, P. Manohar, E. Mansoor, S. F. Manzer, S.-P. Mao, A. V. Marenich, T. Markovich, S. Mason, S. A. Maurer, P. F. McLaughlin, M. F. S. J. Menger, J.-M. Mewes, S. A. Mewes, P. Morgante, J. W. Mullinax, K. J. Oosterbaan, G. Paran, A. C. Paul, S. K. Paul, F. Pavošević, Z. Pei, S. Prager, E. I. Proynov, Á. Rák, E. Ramos-Cordoba, B. Rana, A. E. Rask, A. Rettig, R. M. Richard, F. Rob, E. Rossomme, T. Scheele, R. Scheurer, M. Schneider, N. Sergueev, S. M. Sharada, W. Skomorowski, D. W. Small, C. J. Stein, Y.-C. Su, E. J. Sundstrom, Z. Tao, J. Thirman, G. J. Tornai, T. Tsuchimochi, N. M. Tubman, S. P. Veccham, O. Vydrov, J. Wenzel, J. Witte, A. Yamada, K. Yao, S. Yeganeh, S. R. Yost, A. Zech, I. Y. Zhang, X. Zhang, Y. Zhang, D. Zuev, A. Aspuru-Guzik, A. T. Bell, N. A. Besley, K. B. Bravaya, B. R. Brooks, D. Casanova, J.-D. Chai, S. Coriani, C. J. Cramer, G. Cserey, A. E. DePrince, R. A. DiStasio, A. Dreuw, B. D. Dunietz, T. R. Furlani, W. A. Goddard, S. Hammes-Schiffer, T. Head-Gordon, W. J. Hehre, C.-P. Hsu, T.-C. Jagau, Y. Jung, A. Klamt, J. Kong, D. S. Lambrecht, W. Liang, N. J. Mayhall, C. W. McCurdy, J. B. Neaton, C. Ochsenfeld, J. A. Parkhill, R. Peverati, V. A. Rassolov, Y. Shao, L. V. Slipchenko, T. Stauch, R. P. Steele, J. E. Subotnik, A. J. W. Thom, A. Tkatchenko, D. G. Truhlar, T. Van Voorhis, T. A. Wesolowski, K. B. Whaley, H. L. Woodcock, P. M. Zimmerman, S. Faraji, P. M. W. Gill, M. Head-Gordon, J. M. Herbert, and A. I. Krylov, "Software for the frontiers of quantum chemistry: An overview of developments in the Q-Chem 5 package," *J. Chem. Phys.* **155**, 084801 (2021).
- ⁶³J. P. Perdew, K. Burke, and M. Ernzerhof, "Generalized gradient approximation made simple [Phys. Rev. Lett. **77**, 3865 (1996)]," *Phys. Rev. Lett.* **78**, 1396 (1997).
- ⁶⁴R. A. Kendall, T. H. Dunning, and R. J. Harrison, "Electron affinities of the first-row atoms revisited. Systematic basis sets and wave functions," *J. Chem. Phys.* **96**, 6796–6806 (1992).
- ⁶⁵A. Halkier, H. Koch, O. Christiansen, P. Jørgensen, and T. Helgaker, "First-order one-electron properties in the integral-direct coupled cluster singles and doubles model," *J. Chem. Phys.* **107**, 849–866 (1997).
- ⁶⁶Y. Zhang, A. Otani, and E. J. Maginn, "Reliable viscosity calculation from equilibrium molecular dynamics simulations: A time decomposition method," *J. Chem. Theory Comput.* **11**, 3537–3546 (2015).
- ⁶⁷P. Pyykkö, "Year-2017 nuclear quadrupole moments," *Mol. Phys.* **116**, 1328–1338 (2018).
- ⁶⁸D. Bedrov, J.-P. Piquemal, O. Borodin, A. D. MacKerell, B. Roux, and C. Schröder, "Molecular dynamics simulations of ionic liquids and electrolytes using polarizable force fields," *Chem. Rev.* **119**, 7940–7995 (2019).